

Gain-assisted optical tweezing of plasmonic and large refractive index microspheres

R. Ali^{1,*}, R. S. Dutra², F. A. Pinheiro³ & P. A. Maia Neto³

¹ Applied Physics Department, Gleb Wataghin Physics Institute, University of Campinas, Campinas 13083-859, SP, Brazil

² LISComp-IFRJ, Instituto Federal de Educação, Ciência e Tecnologia, Rua Sebastião de Lacerda, Paracambi, RJ, 26600-000, Brasil

³ Instituto de Física, Universidade Federal do Rio de Janeiro, Caixa Postal 68528, Rio de Janeiro, RJ, 21941-972, Brasil

E-mail: *rali.physicist@gmail.com

Abstract. We have theoretically investigated optical tweezing of gain-functionalized microspheres using a highly focused single beam in the nonparaxial regime. We employ the Mie-Debye theory of optical tweezers to calculate the optical force acting on homogeneous and core-shell Mie microspheres with gain. We demonstrate that the optical gain plays a crucial role in optical manipulation, especially to optimize the restoring force and thus allowing for trapping of large refractive index and plasmonic particles. Indeed we demonstrate that one can trap such particles, which is usually not possible in the case of passive media, by functionalizing them with an optical gain material. We show that by varying the value of the gain, which can be realized by changing the pump power, one can not only achieve trapping but also manipulate the equilibrium position of the tweezed particle. Altogether our findings open new venues for gain-assisted optomechanics, where gain functionalized systems could facilitate optical trapping and manipulation of plasmonic nanoparticles in particular, with potential applications in self-assembling of nanoparticle suspensions and on a chip.

1. Introduction

Since the invention of optical tweezers [1, 2], optical manipulation have experienced notable progress, both scientifically and technologically, with many applications in several areas such as atomic physics, optics and biology [3, 4]. Optical manipulation comprises not only trapping, but also cooling, binding, sorting and transporting [5]. These tasks require controlling both linear and angular momenta of light to achieve tractor beams [6], pulling forces [7, 8, 9, 10], and optical torques at the micro and nanoscale [11, 12, 13, 14], unveiling new aspects of light-matter interactions.

In typical experimental setups of optical tweezers, a single tightly-focused laser beam is used to control the position of a (typically spherical) particle. The exchange of linear momentum upon light reflection by the particle produces a pushing, radiation pressure force. On the other hand, the refraction of a strongly-focused light beam

gives rise to a restoring force bringing the particle to the focal point. Stable trapping is achieved at the point at which the two force components equilibrate [15]. The detrimental radiation pressure effect tends to be dominant in the case of large refractive index, absorbing, and resonant particles. As a result trapping is typically difficult to implement in those cases. Plasmonic particles of sizes larger than the wavelength are important examples as in this case even large numerical aperture (NA) objectives cannot provide restoring forces sufficiently large to compensate for the strong radiation pressure component [16]. Despite challenging, trapping of large metallic particles remains a sought-after effect for practical applications that include spectroscopy, catalysis, micro-fabrication, biotechnology, and medical science [17].

In order to circumvent these limitations, several techniques have been proposed to enhance restoring forces. For instance, optical tweezing can be facilitated and optimized by using anti-reflecting coatings [18, 19]. Additional proposals include suppressing backscattering using composite media to achieve the Kerker condition [20], tailoring the optical properties of the surrounding host medium [21, 22], exciting surface plasmon polaritons in the particle [23, 24, 25], and exploring the optical response of chiral particles illuminated by circularly-polarized beams [26]. All of the aforementioned works consider passive media only.

However, recent progress in nanofabrication techniques has opened the way for the design of gain-functionalized plasmonic nanoparticles, where encapsulated dye molecules are doped in homogeneous and coated metallic spheres, leading not only to loss compensation but also to a strong resonant coupling between the gain medium and the metal [27]. Recent applications of optical manipulation assisted by gain media include tailored optical forces by dual-beams on gain enriched Rayleigh particles [28, 29] and optical pulling forces [30]. Advances in the field of metamaterials also allow to design microspheres with optical gain [31, 32], with several applications [33, 34, 35].

In this paper, we investigate optical tweezing of gain-functionalized spherical particles, including core-shell plasmonic structures, using a single tightly focused laser beam. We demonstrate that optical gain plays a crucial role to facilitate and optimize trapping of plasmonic and large spheres with high refractive indexes, which cannot be trapped by a single focused beam without the assistance of gain. We systematically show that a moderate amount of gain allows for stable trapping. We consider three different realistic structural morphologies: homogeneous microspheres and core-shell particles with either a dielectric or plasmonic core and a dye-doped shell. For each configuration, we identify the corresponding lowest and the highest value of gain that differentiate the regions where optical trapping and optical pulling occur. We also demonstrate how the trapping position depends on the gain value, which can be adjusted dynamically by varying the pump power.

2. Methodology

In a typical optical tweezers setup, a single incident laser beam is strongly focused

by a high numerical aperture (NA) objective lens producing a non-paraxial beam in the sample region, which contains an aqueous suspension (refractive index $n_w = \sqrt{\epsilon_w}$) of spherical particles. For simplicity, we consider an aplanatic (aberration-free) trapping beam. An extension to include optical aberrations can be implemented along the lines of Ref. [36]. The electric field representing the focused laser beam is written as a superposition of plane waves as follows [37]

$$\mathbf{E}_{\text{in}}(\mathbf{r}) = E_0 \int_0^{2\pi} d\varphi_k \int_0^{\theta_0} d\theta_k \sin \theta_k \sqrt{\cos \theta_k} e^{-\gamma_f^2 \sin^2 \theta_k} \times e^{i\mathbf{k}(\theta_k, \varphi_k) \cdot (\mathbf{r} + \mathbf{r}_s)} \hat{\mathbf{x}}'(\theta_k, \varphi_k), \quad (1)$$

where the direction of the wave vector $\mathbf{k}(\theta_k, \varphi_k)$ is defined by the angular spherical coordinates (θ_k, φ_k) . The region of integration in Fourier space is defined by the semi-aperture angle $\theta_0 = \sin^{-1}(\text{NA}/n_w)$ if $\text{NA}/n_w \leq 1$ and $\theta_0 = \pi/2$ otherwise. All Fourier components share the same modulus $|\mathbf{k}| = n_w \omega/c$ where ω is the angular frequency and c is the speed of light in vacuum. We assume that the Gaussian laser beam at the objective entrance port (beam waist w) is linearly-polarized along the x -direction. The unit vector $\hat{\mathbf{x}}'(\theta_k, \varphi_k)$ is obtained from $\hat{\mathbf{x}}$ by rotation with Euler angles $\alpha = \varphi_k$, $\beta = \theta_k$ and $\gamma = -\varphi_k$. We also define $\gamma_f = f/w$ where f is the objective focal length. Finally, we set the origin at the center of the sphere and the focal point is at position $-\mathbf{r}_s$.

We take $\mathbf{E}_{\text{in}}(\mathbf{r})$ as the incident field on the the spherical particle to be trapped. The Mie-Debye theory of optical tweezers [38, 39, 40] combines Mie scattering with the Debye-type non-paraxial integral representation (1) for the focused trapping beam. Each Fourier component of \mathbf{E}_{in} is scattered by the particle according to the Mie formalism [41]. The resulting scattered field can be written with the help of Wigner finite rotation matrix elements $d_{m,m'}^{\ell}(\theta)$ [42]. We then compute the optical force \mathbf{F} by integrating the Maxwell stress tensor over a spherical Gaussian surface $S(r)$ of radius $r \rightarrow \infty$:

$$\mathbf{F} = \lim_{r \rightarrow \infty} \left[-\frac{r}{2} \int_{S(r)} d\Omega \mathbf{r} (\epsilon_0 \epsilon_w E^2 + \mu_0 H^2) \right]. \quad (2)$$

Here, \mathbf{E} and \mathbf{H} are the total electric and magnetic fields, and ϵ_0 and μ_0 denote the vacuum permittivity and permeability, respectively.

After concluding the formal derivation, we displace the origin to the focal point and represent the position of the sphere center relative to the focus $\mathbf{r}_s(\rho, \phi, z)$ in cylindrical coordinates. For sake of convenience, we define the normalized, dimensionless optical force efficiency [15]

$$\mathbf{Q}(\rho, \phi, z) = \frac{\mathbf{F}(\rho, \phi, z)}{n_w P/c},$$

where P is the laser beam power at the sample region. The axial (Q_z) and radial (Q_ρ) cylindrical components are of particular interest. The former provides information on trap stability along the z axis, which is usually the most difficult direction due to the detrimental effect of radiation pressure. To this end, the trapping of a passive sphere occurs due to the interplay between the gradient and radiation pressure forces, where the former points towards the beam focus while the latter points along the positive laser

beam axis regardless of the particle's position. Since the radiation pressure along any radial direction is negligible, the larger gradient force always provides stable trapping on the xy plane. However, when considering a particle with gain, photons are emitted along one of the directions defined by the Fourier decomposition of the incident beam, as given by (1). If the particle is slightly displaced off-axis, the recoil effect provides an outward force component on the xy plane. Thus, the stability on the xy plane might also be in question when considering gain. Hence it is important to calculate the transverse stiffness (z_{eq} = equilibrium position)

$$\kappa_\rho = -\frac{n_w P}{c} \frac{\partial Q_\rho}{\partial \rho} \Big|_{\rho=0}^{z=z_{\text{eq}}}, \quad (3)$$

as stable three-dimensional trapping is only achieved when the condition $\kappa_\rho > 0$ is also met in addition to the requirement of axial trap stability defined by Q_z . We take the x direction corresponding to the linear polarization of the laser beam at the objective entrance port when calculating the derivative in Eq. 3, since it corresponds to the direction of weaker confinement on the xy plane as the focused spot is elongated along the incident polarization direction [37].

2.1. Optical gain model

Optical gain media may be achieved for instance by doping the dielectric media with dye molecules (e.g. rhodamine) or solid-state emitters, such as quantum dots or nitrogen vacancy centers in diamond. For our purposes, we take the vacuum wavelength $\lambda = 1.064 \mu\text{m}$ and $n_w = 1.332$ for the refractive index of the aqueous medium hosting the microspheres. The microsphere is filled by an active medium of complex refractive index $n_p = \text{Re}(n_p) + i \text{Im}(n_p)$ with $\text{Im}(n_p) < 0$. Such condition could be implemented by doping a dielectric material with dye molecules or quantum dots. For instance, one can dope a dielectric medium of relative permittivity ϵ_h with four-level dye molecules. The resulting relative permittivity can be modeled by the dispersion relation [29, 28, 32]

$$\epsilon_p(\omega) = \epsilon_h(\omega) - \frac{N_{\text{dye}} \mu^2}{3\hbar\epsilon_0} \frac{\tilde{N}}{(\omega - \omega_a) + i/\tau}, \quad (4)$$

where \hbar denotes the reduced Planck constant. The dye concentration is represented by the number density N_{dye} and \tilde{N} is the population inversion coefficient: $\tilde{N} = 0$ when the molecules are in the ground state and $\tilde{N} = 1$ for a fully inverted population. The remaining parameters appearing in (4) characterize the dye molecule: τ is the relaxation time, μ is the amplitude of the transition dipole moment, and ω_a is the emission frequency.

In the numerical examples discussed below, we consider realistic values for the gain level $\text{Im}(n_p) < 0$ that can be achieved by choosing the appropriate dye concentration N_{dye} or by tuning the power of a pump laser beam driving the population inversion \tilde{N} . Figure 1 shows a density plot of (a) $\text{Re}(n_p)$ and (b) $\text{Im}(n_p)$ as functions of N_{dye} and \tilde{N} , as calculated from 4. For concreteness, we take the example of a silica host medium

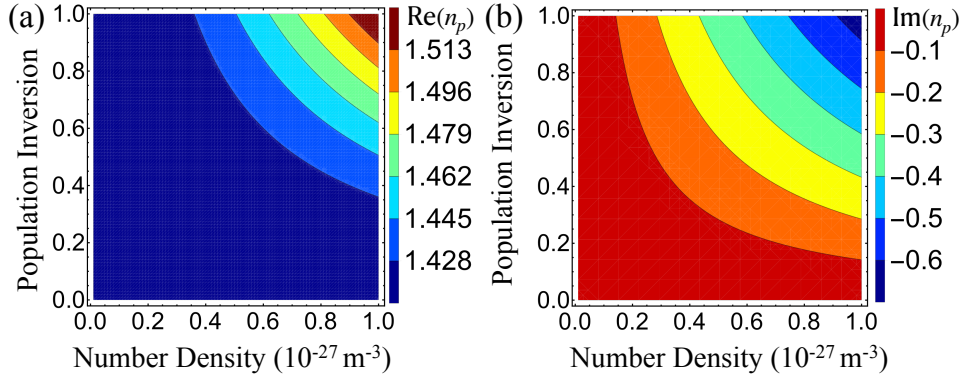


Figure 1. (a) Real and (b) imaginary parts of the refractive index $n_p = \sqrt{\epsilon_p}$ of a gain medium as functions of the number density of dye molecules N_{dye} and the population inversion \tilde{N} . We consider silica as the host medium and take the parameters corresponding to the molecule solvatochromic dye LDS 798 [43]: $\omega_a = 1.77 \times 10^{15}$ Hz, $\mu = 1.33 \times 10^{-29}$ C m and $\tau = 5 \times 10^{-15}$ s.

doped with the molecule solvatochromic dye LDS 798 [43], whose parameters are given by Refs. [29, 28].

3. Results and discussion

In Fig. 2, we consider a homogenous microsphere of radius $R = 400$ nm and typical values for the parameters $\text{NA} = 1.4$ and $\gamma_f = 0.667$ [36]. In panel (a), we plot the axial force efficiency Q_z as a function of $\text{Re}(n_p)$ for $\text{Im}(n_p) = 0$ (solid line), corresponding to a passive, absorptionless particle, and for an active sphere with $\text{Im}(n_p) = -0.05$ (dashed line). We take a fixed position along the beam axis $z/R = 0.2$. We represent the value $n_w = 1.332$ by a vertical dashed line.

The solid line in Fig. 2(a) reveals that for passive spheres optical tweezing can only occur for a narrow range of refractive indexes, namely $n_w < \text{Re}(n_p) \lesssim 1.92$, since axial trapping requires a restoring negative axial force. Indeed, when $\text{Re}(n_p) < n_w$ the polarizability becomes negative and then the particle is expelled from the focal region. On the other hand, for large indexes outside the trapping range, radiation pressure becomes dominant as reflection overcomes refraction, which also prevents trapping.

However, trapping is facilitated when the microsphere with the same $\text{Re}(n_p)$ and radius is doped with a gain material. As indicated by the dashed line in Fig. 2(a), trapping can now be achieved over a much broader range of refractive indexes, as indicated by the range leading to negative optical forces. This is a consequence of the recoil arising from stimulated emission along directions close to the positive z direction, thus leading to a net backward force.

In addition to the stability along the z axis, we also investigate the transverse trap stiffness on the xy plane to verify three-dimensional stability of the optical trap. We plot κ_ρ as a function of $\text{Re}(n_p)$ in Fig. 2(b), with the same conventions employed in panel (a). The plot shows that the equilibrium position along the axis is unstable

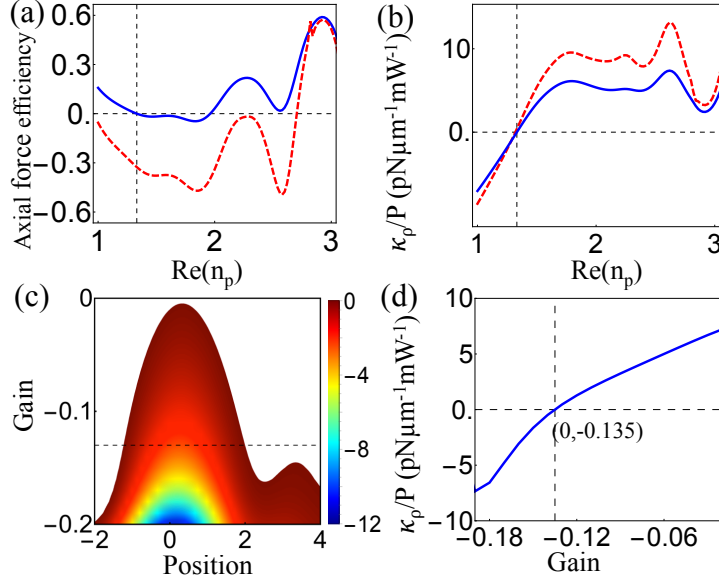


Figure 2. Optical force on a homogenous gain-enriched microsphere. (a) Normalized axial force Q_z and (b) transverse trap stiffness κ_ρ (divided by the local power) as functions of the real part of the microsphere’s refractive index: passive absorptionless (solid) and gain functionalized (dash) with $\text{Im}(n_p) = -0.05$. The vertical lines indicate the refractive index $n_w = 1.332$ of the aqueous immersion medium. (c) Density plot of Q_z as function of position (in units of radius) along the beam axis and of $\text{Im}(n_p)$ for $\text{Re}(n_p) = 2.6$. The horizontal dashed line indicates the critical value $\text{Im}(n_p) = -0.135$. Only negative values of Q_z , which correspond to a backward force, are shown. (d) Transverse trap stiffness κ_ρ as function of $\text{Im}(n_p)$, again with $\text{Re}(n_p) = 2.6$. The vertical dashed line indicates the critical gain $\text{Im}(n_p) = -0.135$, above which stability on the xy plane is lost.

when the refractive index is lower than the refractive index of the surrounding medium (dashed vertical line), corresponding to a negative polarizability. Thus, there is no three-dimensional trapping in this case even when one considers gain. On the other hand, the presence of gain indeed allows for trapping of high refractive index particles. Indeed, as $\kappa_\rho > 0$ in this case, the maximum value of $\text{Re}(n_p)$ allowing for trapping is solely determined by the condition for stability along the axis, which was discussed in connection with panel (a).

Next, we unveil the role of gain in optical tweezing by analyzing the variation of the optical force with the gain parameter $\text{Im}(n_p)$ for a fixed $\text{Re}(n_p) = 2.6$. In Fig. 2(c), we plot the axial force efficiency Q_z as a function of position along the z -axis (in units of radius) and of the gain parameter $\text{Im}(n_p)$. The plot reveals that a very small amount of gain is sufficient to allow for tweezing of a high-index particle. The stable equilibrium position as a function of gain is given by the lefthand boundary of the colored region. In the case of passive microspheres interacting with aplanatic focused beams, the trapping position is always above focus (positive z -axis) [38, 39], as it results from the equilibrium between the positive radiation pressure and the negative (backward) force component pointing to the focus and responsible for trapping [15]. Here, however, the equilibrium

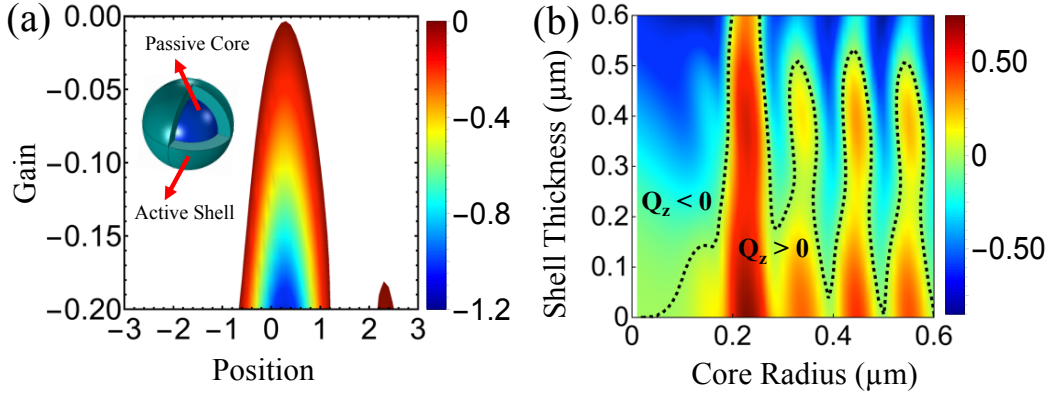


Figure 3. Optical force on a core-shell particle with a dielectric core and a gain-enriched shell. (a) Density plot of the normalized axial force efficiency Q_z as a function of axial position (in units of outer radius) and gain. Only negative values are indicated. The core radius is $R_c = 400$ nm and the shell thickness is $t = 200$ nm. (b) Density plot of Q_z as a function of R_c and t . We fix the position at $z/(R_c + t) = 0.1$ and consider the gain parameter $\text{Im}(n_p) = -0.05$. The dotted line corresponds to $Q_z = 0$.

position is located below the focal plane (negative z) because of the recoil effect leading to a negative force even below focus. Figure 2(c) shows that the particle's equilibrium position can be controlled by changing the gain parameter, which can be achieved with a negligible variation of $\text{Re}(n_p)$ by changing, for instance, the pump power driving the population inversion \tilde{N} as indicated in Fig. 1. As expected, the trapping position is displaced further below focus as the gain increases.

However, when the gain parameter increases past the threshold value indicated by the horizontal dashed line in Fig. 2(c), the equilibrium position becomes unstable on the xy plane. This is indicated by panel (d), showing that the transverse trap stiffness κ_ρ (in units of power) goes negative for $\text{Im}(n_p) < -0.135$. Panels (c) and (d) reveal a transition from a trapping regime to an optical pulling one as the gain increases, with the z -axis becoming unstable as the effect of recoil becomes more dominant.

After demonstrating that gain facilitates optical trapping and manipulation of homogeneous microspheres, we now consider gain functionalized core-shell particles, which can be nanofabricated by chemically encapsulating dye molecules in the shell [27]. By adding the geometric aspect ratio to the parameter space, the core-shell configuration provides a richer variety of applications and physical effects, as discussed in the following.

As a realistic example, we consider a coated microsphere composed of a dielectric core of refractive index $n_c = 2.6$ and a dye-doped nanoshell of refractive index $n_s = 1.44 + \text{Im}(n_s)$. Figure 3(a) presents a density plot of Q_z as a function of axial position and gain parameter $\text{Im}(n_s)$. We consider a core of radius $R_c = 400$ nm and a shell of thickness $t = 200$ nm. Only the regions with negative values of Q_z , allowing for trapping, are shown. As in the case of homogeneous microspheres, a very small amount of gain is sufficient to allow for trapping of particles with a high-index core. In addition, one can not only displace the trapping position downstream by increasing the gain but

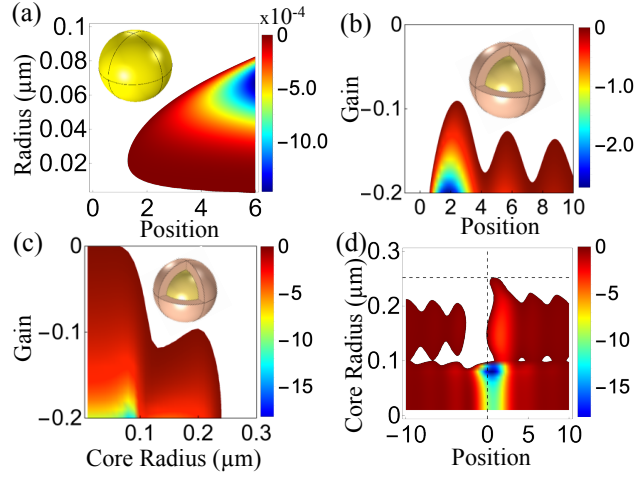


Figure 4. Optical force on metallic particles in vacuum. (a) Homogeneous gold particle: Normalized axial force efficiency Q_z as a function of axial position and radius. Core-shell particle with gold core and gain-enriched shell: Q_z as a function of (b) axial position and gain parameter $\text{Im}(n_s)$, with core radius $R_c = 200$ nm shell thickness $t = 300$ nm; (c) core radius and gain parameter at axial position $z/(R_c + t) = 2$; (d) axial position and core radius with gain $\text{Im}(n_s) = -0.2$. In panels (b), (c) and (d), the outer radius is $R_c + t = 500$ nm. Only negative values of Q_z are shown and the axial position is measured in units of the outer radius.

also achieve multiple equilibria [44]. Indeed, Fig. 3(a) shows that a second equilibrium position appears at $z = 2.2(R_c + t)$, which is, however, only marginally stable.

In order to elucidate the role of geometric parameters of the core/shell particle, Fig. 3 (b) presents a density plot of Q_z as a function of the core radius R_c and shell thickness t for the fixed axial position $z = 0.1(R_c + t)$. We fix the gain parameter at $\text{Im}(n_s) = -0.05$ and otherwise take the same parameters of 3(a). The dotted line, corresponding to $Q_z = 0$, represents the boundary separating the region allowing for optical tweezing ($Q_z < 0$) from the one where radiation pressure dominates and precludes trapping. In all cases with $Q_z < 0$ in Fig. 3, we verify that $\kappa_\rho > 0$ so that three-dimensional trapping is possible.

As a third example, we now examine the case where the core is metallic, as in the nano-fabrication reported by Ref. [27]. In general, trapping of metallic spheres is difficult due to the dominant role of radiation pressure. In addition, strong absorption leads to detrimental radiometric effects when considering an aqueous suspension. To avoid the presence of thermal effects, from now on we assume that the external medium is vacuum. For consistency, we then consider a dry objective with $\text{NA} = 0.95$. As an example, we take a homogenous gold nanoparticle with refractive index $n_g = 0.25 + 6.96i$. We plot the axial efficiency Q_z as function of axial position and radius in Fig. 4(a). The panel shows that backward forces and trapping are only achieved for very small particles, in the regime of validity of the Rayleigh (electric dipole) approximation.

The size range allowing for trapping of metallic particles can be significantly

enlarged by coating the metallic core with a gain medium, as illustrated by panel (b) of Fig. 4, showing Q_z as a function of axial position (in units of outer radius) and gain parameter $\text{Im}(n_s)$ for core radius $R_c = 200$ nm and shell thickness $t = 300$ nm. Here, the refractive index of the shell is $n_s = 1.44 + \text{Im}(n_s)$, while the refractive index of the gold core is the same as in panel (a). The minimum gain $\text{Im}(n_s) \approx -0.09$ required for trapping is much larger than in the examples considered previously, but still within reach with realistic parameters for the dye doping as indicated by Fig. 1. Indeed, in the case of metallic particles, a larger gain is required to compensate for the stronger radiation pressure arising from the enhanced backward scattering and absorption.

Figure 4(b) shows that the equilibrium position can be manipulated by changing the gain, as in the systems considered in Figs. 2 and 3. In contrast to the previous configurations, however, equilibrium is achieved above the focal plane because of the larger contribution of radiation pressure, and the particle position approaches the focal point from above as the gain increases. Multiple stable equilibria appear at intermediate values of the gain parameter. As the gain is further increased, the separate potential wells merge into a single, deeper well. More generally, when comparing the results of panel (b) with those of panel (a), it is worth noticing that the backward negative force increases by roughly four orders of magnitude as the plasmonic resonances of the gold core are enhanced by the externally pumped energy associated with gain in the shell region.

As the metallic core radius R_c increases, so does the detrimental radiation pressure, making it increasingly harder to trap with a single laser beam. According to Fig. 4(c), showing the variation of Q_z with R_c and $\text{Im}(n_s)$ at the axial position $z/(R_c + t) = 2$ for $R_c + t = 500$ nm, the largest core allowing for trapping with this arrangement corresponds to $R_c = 252$ nm at the gain parameter $\text{Im}(n_s) = -0.2$.

We analyze how the core size modifies the optical force along the z -axis for such value of gain in Fig. 4(d). As the core radius decreases from the maximum value $R_c = 252$ nm, the range of positions allowing for a restoring backward force expands and develops multiple equilibria for radii slightly above $0.2 \mu\text{m}$. The plot shows that multiple equilibria also appear below focus (negative z) as the radius is further reduced, and then a pulling range develops since the radiation pressure associated to the core becomes increasingly subdominant in comparison with the recoil effect. Indeed, Fig. 4(d) reveals a crossover between optical tweezing and optical pulling [7] as R_c decreases. Both effects are characterized by a negative force, but the latter corresponds to a pulling towards the laser source without defining any equilibrium position. Such pulling range is first confined to the region below focus for $R_c \approx 0.15 \mu\text{m}$, and then expands into the entire space as the core radius is reduced below $0.1 \mu\text{m}$.

In contrast to the case of homogenous dielectric microspheres discussed in connection with Fig. 2, here the pulling regime preserves stability on the xy -plane, since the transverse stiffness κ_ρ remains positive in all cases leading to negative forces in Fig. 4. Thus, as the particle is pulled towards the laser source, it is also attracted to the beam symmetry axis.

System	Pulling force	Multiple stable points	Minimum gain for trapping
Homogeneous sphere with gain	No	No	10^{-3}
Dielectric core / gain shell	No	Marginal	10^{-3}
Metal core / gain shell	Yes	Yes	10^{-1}

Table 1. Table summarizing the main functionalities that may be achieved with the different gain nanoparticles discussed in this work.

4. Conclusions

In conclusion, we present a systematic study of optical tweezing in the presence of gain functionalized microspheres using a single focused beam. We consider several realistic examples of practical interest including gain enriched homogeneous microspheres and hybrid core/shell plasmonic nanoparticles. We demonstrate that the presence of gain allows for optical trapping in a wide variety of systems that usually cannot be employed in optical tweezers, including plasmonic and large refractive index particles. In these cases we show that the trapping conditions strongly depend of the gain value, including the equilibrium position of the trapped particle, which could be externally controlled by varying the pump power at realistic conditions. We also demonstrate a crossover between pulling forces and optical forces leading to stable optical tweezing, as summarized in Table 1. Altogether, our findings set the grounds for the incorporation of gain in optical tweezers, expanding their employment to new systems such as plasmonic and large, high refractive microparticles, with many potential applications such as self-assembling and gain-assisted optomechanics.

5. Acknowledgements

We thank S. Iqbal, G. Wiederhecker and F. S. S. da Rosa for inspiring discussions. We acknowledge funding from the Brazilian agencies Conselho Nacional de Desenvolvimento Científico e Tecnológico (CNPq), Coordenação de Aperfeiçoamento de Pessoal de Nível Superior (CAPES), Instituto Nacional de Ciência e Tecnologia de Fluidos Complexos (INCT-FCx), Fundação de Amparo à Pesquisa do Estado do Rio de Janeiro (FAPERJ) (202.874/2017 and 210.242/2018) and Fundação de Amparo à Pesquisa do Estado de São Paulo (FAPESP) (2014/50983-3 and 2020/03131-2).

6. References

- [1] A. Ashkin, J. M. Dziedzic, J. E. Bjorkholm, and S. Chu, Observation of a single-beam gradient force optical trap for dielectric particles, *Opt. Lett.* **11**, 288 (1986).
- [2] A. Ashkin, J. M. Dziedzic, Optical trapping and manipulation of viruses and bacteria, *Science*, **235**, 1517 (1987).

- [3] A. Ashkin, Optical trapping and manipulation of neutral particles using lasers: A reprint volume with commentaries (World Scientific, Singapore, 2006).
- [4] P. Polimeno, A. Magazzù, M. A. Iatì, *et al.*, Optical tweezers and their applications, *J. Quant. Spectrosc. Radiat. Transf.* **218**, 131 (2018).
- [5] D. Gao, W. Ding, M. Nieto-Vesperinas, *et al.*, Optical manipulation from the microscale to the nanoscale: fundamentals, advances and prospects, *Light Sci, Appl.* **6**, e17039 (2017).
- [6] S. Sukhov and A. Dogariu, Negative nonconservative forces: optical “tractor beams” for arbitrary objects, *Phys Rev. Lett.* **107**, 20360 (2011).
- [7] J. Chen, J. Ng, Z. Lin, and C. T. Chan, Optical pulling force, *Nature Photon.* **5**, 531 (2011).
- [8] A. Dogariu, S. Sukhov, and J. J. Sáenz. Optically induced negative forces, *Nat. Photon.* **7**, 24 (2013).
- [9] R. Ali, F. A. Pinheiro, R. S. Dutra, and P. A. M. Neto, Tailoring optical pulling forces with composite microspheres, *Phys. Rev. A* **102**, 023514 (2020).
- [10] R. Ali, R. S. Dutra, F. A. Pinheiro, and P. A. Maia Neto, Enantioselection and chiral sorting of single microspheres using optical pulling forces, *Opt. Lett.* **46**, 1640 (2021).
- [11] D. G. Grier, A revolution in optical manipulation, *Nature* **424**, 810 (2003).
- [12] D. B. Ruffner, and D. G. Grier, Optical Forces and Torques in Nonuniform Beams of Light, *Phys. Rev. Lett.* **108**, 173602 (2012).
- [13] K. Diniz, R. S. Dutra, L. B. Pires, N. B. Viana, H. M. Nussenzveig, and P. A. Maia Neto, Negative optical torque on a microsphere in optical tweezers, *Opt. Express* **27**, 5905-5917 (2019).
- [14] R. Ali, F. A. Pinheiro, F. S. S. Rosa, R. S. Dutra, and P. A. Maia Neto, Enantioselective manipulation of chiral nanoparticles using optical tweezers, *Nanoscale*, **12**, 5031 (2020).
- [15] A. Ashkin, Forces of a single-beam gradient laser trap on a dielectric sphere in the ray optics regime, *Biophysical J.* **61**, 569 (1992).
- [16] C. Min, Changjun, *et al.*, Focused plasmonic trapping of metallic particles, *Nature Comm* **4**, 1 (2013).
- [17] Y. Zhang, X. Dou, Y. Dai, X. Wang, C. Min, and X. Yuan, All-optical manipulation of micrometer-sized metallic particles, *Photon. Res.* **6**, 66 (2018).
- [18] D. Craig, A. McDonald, M. Mazilu, H. Rendall, F. Gunn-Moore, and K. Dholakia, Enhanced optical manipulation of cells using antireflection coated microparticles, *ACS Photonics* **2**, 1403 (2015).
- [19] N. Wang, X. Li, J. Chen, Z. Lin, and J. Ng, Gradient and scattering forces of anti-reflection-coated spheres in an aplanatic beam, *Sci. Rep.* **8**, 17423 (2018)
- [20] R. Ali, F. A. Pinheiro, F. S. S. Rosa, R. S. Dutra, and P. A. Maia Neto, Optimizing optical tweezing with directional scattering in composite microspheres, *Phys. Rev. A* **98**, 053804 (2018).
- [21] O. M. Marago, P. H. Jones, F. Bonaccorso, V. Scardaci, P. G. Gucciardi, A. G. Rozhin, and A. C. Ferrari, Femtonewton force sensing with optically trapped nanotubes, *Nano Lett.* **8**, 3211 (2008).
- [22] R. Ali, R.S. Dutra, F. A. Pinheiro, R. S. S. Rosa, and P. A. Maia Neto, Theory of optical tweezing of dielectric microspheres in chiral host media and its applications, *Sci. Rep.* **10**, 16481 (2020).
- [23] G. Volpe, R. Quidant, G. Badenes, and D. Petrov, Surface plasmon radiation forces, *Phys. Rev. Lett.* **96**, 238101 (2006).
- [24] C. Min, Z. Shen, J. Shen, Y. Zhang, H. Fang, G. Yuan, L. Du, S. Zhu, T. Lei, and X. Yuan, Focused plasmonic trapping of metallic particles, *Nat. Commun.* **4**, 2891 (2013).
- [25] O. Brzobohatý, *et al.* Three-dimensional optical trapping of a plasmonic nanoparticle using low numerical aperture optical tweezers, *Sci. Rep.* **5**, 8106 (2015).
- [26] R. Ali, F. A. Pinheiro, R. S. Dutra, F. S. S. Rosa, and P. A. Maia Neto, Probing the optical chiral response of single nanoparticles with optical tweezers, *J. Opt. Soc. Am. B* **37**, 2796 (2020).
- [27] A. De Luca, *et al.*, Gain functionalized core-shell nanoparticles: the way to selectively compensate absorptive losses, *J. Mater. Chem.* **22**, 8846 (2012).
- [28] L. Pezzi, M. Antonia Iatí, R. Saija, A. De Luca, and O. M. Maragó, Resonant coupling and gain

- singularities in detal/dielectric multishells: quasi-static versus T-matrix calculations, *J. Phys. Chem. C*, **123**, 29291 (2019).
- [29] P. Polimeno, F. Patti, M. Infusino, J. Sánchez, M. A. Iatí, R. Saija, G. Volpe, O. M. Marago, and A. Veltri, Gain-assisted optomechanical position locking of metal/dielectric nanoshells in optical potentials, *ACS Photonics*, **7**, 1262 (2020).
- [30] X. Bian, D. L. Gao, and L. Gao, Tailoring optical pulling force on gain coated nanoparticles with nonlocal effective medium theory, *Opt. Express* **25**, 24566 (2017).
- [31] A. D. Boardman V. V. Grimalsky Y. S. Kivshar S.V. Koshevaya M. Lapine N. M. Litchinitser V. N. Malnev M. Noginov Y. G. Rapoport V. M. Shalaev, Active and tunable metamaterials, *Laser & photonics reviews* **5**, 287 (2011).
- [32] S. Campione, M. Albani, and F. Capolino, Complex modes and near-zero permittivity in 3D arrays of plasmonic nanoshells: loss compensation using gain [Invited], *Opt. Mater. Express* **1**, 1077 (2011).
- [33] F. Shen, N. An, Y. Tao, H. Zhou, Z. Jiang, and Z. Guo Anomalous forward scattering of gain-assisted dielectric shell-coated metallic core spherical particles *Nanophotonics* **6**, 1063 (2017).
- [34] J. Olmos-Trigo, and C. Fernández, Kerker conditions upon lossless, absorption, and optical gain regimes, *Phys. Rev. Lett.* **125**, 073205 (2020).
- [35] A. Mizrahi, and Y. Fainman, Negative radiation pressure on gain medium structures, *Opt. Lett.* **35**, 3405 (2010).
- [36] R. S. Dutra, N. B. Viana, P. A. Maia Neto, and H. M. Nussenzveig, Absolute calibration of forces in optical tweezers, *Phys. Rev. A* **90**, 013825 (2014).
- [37] B. Richards, and E. Wolf, Electromagnetic diffraction in optical systems II. Structure of the image field in an aplanatic system, *Proc. R. Soc. London A* **253**, 358 (1959).
- [38] P. A. Maia Neto, and H. M. Nussenzveig, Theory of optical tweezers, *Europhys. Lett.* **50**, 702 (2000).
- [39] A. Mazolli, P. A. Maia Neto, and H. M. Nussenzveig, Theory of trapping forces in optical tweezers, *Proc. R. Soc. Lond. A*, **459**, 3041 (2003).
- [40] R. S. Dutra, N. B. Viana, P. A. M. Neto, and H. M. Nussenzveig, Polarization effects in optical tweezers, *J. Opt. A* **9**, 221 (2007).
- [41] C. F. Bohren, and D. R. Huffman, *Absorption and scattering of light by small particles* (Wiley, New York, 1998).
- [42] A. R. Edmonds, *Angular momentum in quantum mechanics* (Princeton University Press, Princeton, 1957).
- [43] H. Doana, M. Castillob, M. Bejjanic, Z. Nurekeyeva, S. V. Dzyubab, I. Gryczynskid, Z. Gryczynskia, and S. Raut, Solvatochromic dye LDS 798 as microviscosity and pH probe, *Phys. Chem. Chem. Phys.* **19**, 29934 (2017).
- [44] N. B. Viana, M. S. Rocha, O. N. Mesquita, A. Mazolli, P. A. Maia Neto, and H. M. Nussenzveig, Towards absolute calibration of optical tweezers, *Phys. Rev. E.* **75**, 021914 (2007)